JOURNAL OF SPACECRAFT AND ROCKETS
Vol. 40, No. 3, May–June 2003

Hypersonic Flight Transition Data Analysis Using Parabolized Stability Equations with Chemistry Effects

Mujeeb R. Malik*
High Technology Corporation, Hampton, Virginia 23666

Analysis of boundary-layer transition data from supersonic quiet tunnels, as well as flight experiments has indicated that, in the absence of surface roughness and high levels of freestream disturbances, linear stability theory can be used as a guide for estimation of the onset of transition. Transition data from two different hypersonic flight experiments are analyzed using parabolized stability equations, including chemistry effects associated with high-temperature boundary layers. The results suggest that transition in both of these cases is caused by the amplification of second mode disturbances. The analysis shows that, consistent with previous findings for supersonic flows where first mode disturbances induce laminar-turbulent transition, N factors of about 9.5 and 11.2 correlate the transition onset locations from these two high-Mach-number experiments. Therefore, the e^N method can be used for smooth body transition prediction in hypersonic vehicle design. The effect of chemistry on boundary-layer stability is also studied and is shown to be destabilizing.

Nomenclature

c	=	species concentration
M	=	Mach number
p	=	pressure, N/m^2
s	=	surface distance, m
T	=	temperature, K
u	=	boundary-layer velocity, m/s
u_1, u_2, u_3	=	velocity components in (x_1, x_2, x_3) directions
x	=	axial distance, m
x_1, x_2, x_3	=	streamwise, azimuthal, and wall-normal coordinate system
y	=	boundary-layer wall-normal coordinate, m
α	=	nondimensional streamwise wave number
β	=	nondimensional spanwise (azimuthal) wave number
δ	=	boundary-layer thickness, m
λ	=	disturbance wavelength, m
ρ	=	density, kg/m^3
ω	=	nondimensional disturbance frequency

Subscripts

e	=	boundary-layer edge
i	=	a particular species, $1 < i \leq N_s$
w	=	wall
0	=	stagnation
∞	=	freestream

Superscripts

–	=	mean value
$'$	=	perturbation
$\wedge$	=	shape function

Introduction

BOUNDARY-LAYER transition affects almost all aspects of vehicle design due to the highly integrated nature of such vehicles. The greatest system impact occurs due to increased aerodynamic heating by turbulent boundary layers. Higher heating requires more exotic thermal protection systems, which weigh more and are generally more expensive. Boundary-layer transition also affects vehicle drag. For hypersonic vehicles capable of flight, turbulent skin friction may contribute up to about 30% of the overall vehicle drag. Therefore, clever designs that exploit natural laminar flow become highly attractive. Because the airbreathing engine efficiency drops with Mach number, boundary-layer transition becomes a critical design parameter because its location determines the positive (or negative) payload carried by the vehicle. In fact, such is the impact of transition location on hypersonic vehicles that the conceptual design of the now defunct National Aerospace Plane (NASP) was changed from a conelike body to a flat forebody because the latter offered higher transition Reynolds numbers.

Transition is an initial boundary value problem, and its prediction as such requires the identification and prescription of the freestream disturbance field, quantitative understanding of the receptivity to external disturbances (including interaction with wall roughness and surface irregularities), as well as linear and nonlinear amplification of the internalized disturbances [in the form of Tollmien–Schlichting (TS) waves, Gortler vortices, or crossflow waves] by the boundary layer before breakdown to turbulent flow. However, from low-speed experience, and because much of the process involves linear amplification, it has been found that when transition takes place in a low disturbance environment, its location may be correlated using linear stability theory in conjunction with the e^N method. The value of N is obtained by comparing with the experimental data for the onset of transition. The e^N method, first used by Smith and Gamberoni,[1] has been found to work for a wide class of flows that involve TS waves, crossflow disturbances, and Gortler vortices as the primary instability mechanisms. (See for example, Malik.[2])

The application of the e^N method to high-speed flows requires the consideration of all of the possible modes of instability in compressible boundary layers. The stability of the compressible flat-plate boundary layer has been studied by many authors. (See, for example, Lees and Lin[3] and Mack.[4,5]) There are two important modes of instability present in a compressible flat-plate boundary layer. The first mode is an extension to high speeds of the TS instability, though for supersonic Mach numbers it differs in the sense that it is most amplified when oblique. This mode represents viscous instability at low Mach numbers, but the inviscid nature of the instability begins to dominate when Mach number increases because compressible flat-plate boundary-layer profiles contain a generalized inflection point [that is, $\mathrm{d}/\mathrm{d}y(\rho \mathrm{d}u/\mathrm{d}y) = 0$ at some point in the boundary layer]. This mode may be stabilized by wall cooling, suction, and a favorable pressure gradient. The second mode is the

Received 28 May 2002; revision received 12 January 2003; accepted for publication 18 January 2003.

*Chief Scientist. Associate Fellow AIAA.

result of an inviscid instability present due to a region of supersonic mean flow relative to the disturbance phase velocity. The second mode becomes important at Mach numbers above about four, and it has growth rates much higher than the first mode. The existence of both the first and second modes was established in the experiments of Kendall,[6] Demetriades,[7] and Stetson et al.[8] The second mode is different in character from the first mode; it is most amplified when it is two-dimensional and is destabilized with wall cooling.[4,5] It was found by Malik[9] that this mode can be stabilized both with wall suction and favorable pressure gradients. Adverse pressure gradients have been shown to destabilize second mode disturbances.[10] Because the second mode may be considered as a trapped acoustic disturbance, recent theoretical and experimental work by Fedorov et al.[11] has shown that it can be stabilized by wall porosity.

The work of Chen et al.[12] demonstrated the profound impact supersonic wind-tunnel noise can have on laminar/turbulent transition. In the case of supersonic quiet wind tunnels and flight experiments, Malik[9,13] showed that N factors in the range of 9–11 provided good correlation for transition onset locations. More recent experiments[14] in a Mach 6 quiet tunnel confirmed similar conclusions[10] for second-mode induced transition. Hence, it is reasonable to assume that the e^N method will provide a reasonable correlation for high-Mach-number flight transition data obtained on smooth bodies.

Associated with high-altitude hypersonic flight experiments are "hot" boundary layers, which require consideration of chemical reactions and possible thermal nonequilibrium. Malik[15] and Malik and Anderson[16] studied real gas effects on hypersonic boundary-layer stability by assuming air to be in thermal and chemical equilibrium. Both equilibrium and finite rate chemistry effects were investigated by Malik[17] and Stuckert and Reed[18] using linear stability theory. Hudson et al.[19] formulated the hypersonic boundary-layer stability problem by assuming both chemical and thermal nonequilibrium. Stuckert and Reed[18] and Hudson et al.[19] compared their results against those obtained by Malik[15] for the benchmark test case of Mach 10 adiabatic flat-plate flow. Malik et al.[20] (see also Ref. 21) used the equilibrium gas linear stability theory to analyze the boundary layer on the Reentry-F cone.[22,23]

The preceding analyses of hypersonic boundary-layer stability employed quasi-parallel approximation. To account for the effect of mean flow variation (that is, nonparallelism), a project was undertaken at High Technology Corp. to develop a parabolized stability equations (PSE) code to investigate boundary-layer stability under equilibrium and finite rate chemistry assumptions. The PSE approach accounts for nonparallel, as well as body curvature effects, in a consistent manner. The new reacting flow PSE code, RFPSE, has been used to analyze experimental data from two high Mach number flight experiments: the Reentry-F cone[22,23] and the cone experiment described by Sherman and Nakamura.[24] The results of these analyses are reported in this paper because hypersonic transition remains of considerable interest for reentry launch vehicles. The need for the analysis of flight transition data was also recognized by Schneider.[25] We first give a brief description of the problem formulation including PSE and issues related to mean flow computation, as well as chemical, thermal, and transport properties utilized in the present analysis. Mean flow and RFPSE results are also presented. Note that the present analysis is only applicable to smooth body transition. The important problem of wall roughness relevant to hypersonic vehicles would require further research before physics-based computational techniques can be utilized for transition prediction.

Problem Formulation

PSE

In the formulation of the physical problem of stability of reacting flows over hypersonic vehicles, we make the assumptions that the flow is in thermal equilibrium and that the component species follow the perfect gas relation and law of partial pressures. In contrast with the perfect gas equations, the governing equations now include species continuity equations. In addition, chemical reactions introduce source terms in the energy equation. The resulting Navier–Stokes equations can be found, for example, in Ref. 26.

We assume a body-fitted coordinate system for the PSE. The coordinate system is rather general and can be nonorthogonal. The mean flow solution from a general Navier–Stokes grid is converted to profiles on a boundary-layer type of surface-normal system by means of an interface program. The body-fitted coordinates used are denoted by (x_1, x_2, x_3) to represent the streamwise, spanwise (or azimuthal), and wall-normal directions, respectively. We perturb the governing Navier–Stokes equations by decomposing the flow variables (for example, velocity), mass concentration, etc., into a mean and a fluctuation quantity, (for example, $u = \bar{u} + u'$, $c_i = \bar{c}_i + c_i'$, etc.). Substituting these perturbed variables into the governing equations, subtracting from it the steady mean flow, and assuming small perturbations, we obtain linearized Navier–Stokes equations for chemically reacting flows. In the PSE approach, we write disturbance quantities, for example, velocity u', as

$$u' = \hat{u}(x_1, x_3)\chi + \text{complex conjugate} \tag{1a}$$

$$\chi = \exp\left\{ i\left[\int_{x_1} \alpha(\xi)\, \mathrm{d}\xi + \beta x_2 - \omega t \right] \right\} \tag{1b}$$

where β is the wave number along a suitably defined spanwise direction, for example, azimuthal direction for a cone, and ω is the disturbance frequency. Also, $\hat{u}$ is the disturbance shape function and α is the associated streamwise (complex) wave number.

We take advantage of the slow variation of the mean flow in the streamwise direction and impose a condition on $\alpha(x_1)$ such that most of the waviness and growth of the disturbance are absorbed into the exponential function χ in Eq. (1b), making the shape function $\hat{u}(x_1, x_3)$ slowly varying with x_1. Hence, terms such as $\hat{u}_{x_1x_1}$ in the governing equation can be dropped, and we arrive at a set of equations in which the only second-order derivatives are those with respect to x_3. These parabolized stability equations may be written as

$$L_1\hat{\phi} + L_2\frac{\partial\hat{\phi}}{\partial x_1} + L_3\frac{\partial\hat{\phi}}{\partial x_3} + L_4\frac{\partial^2\hat{\phi}}{\partial x_3^2} = 0 \tag{2}$$

where $\hat{\phi} = (\hat{p}, \hat{u}_1, \hat{u}_2, \hat{u}_3, \hat{T}, \hat{c}_1, \hat{c}_2, \ldots, \hat{c}_{N_s})^T$ and L_1–L_4 are $(N_s + 5) \times (N_s + 5)$ square matrices. For two-dimensional or axisymmetric disturbances, the order reduces by one. For a perfect gas or equilibrium gas assumption (following Ref. 16), the order of L_1–L_4 is only 5×5 for three-dimensional disturbances and 4×4 for two-dimensional disturbances.

The preceding equations are to be solved subject to the boundary conditions given hereafter for $x_3 = 0$:

$$\hat{u}_1 = \hat{u}_2 = \hat{u}_3 = \hat{T} = 0 \tag{3a}$$

$$\hat{c}_i = 0, \qquad i = 1, \ldots, N_s \tag{3b}$$

for a fully catalytic wall and

$$\frac{\partial\hat{c}_i}{\partial x_3} = 0, \qquad i = 1, \ldots, N_s \tag{3c}$$

for a noncatalytic wall.

Where $x_3 \to \infty$, we have the following:

$$\hat{u}_1 \to 0, \qquad \hat{u}_2 \to 0, \qquad \hat{u}_3 \to 0$$

$$\hat{T} \to 0, \qquad \hat{c}_i (i = 1, \ldots, N_s) \to 0 \tag{3d}$$

We note that in the quasi-parallel problem the $\partial\hat{\phi}/\partial x_1$ term drops out. Matrices L_1–L_4 also simplify because $\bar{u}_3 = \partial\bar{u}/\partial x_1 = \mathrm{d}\alpha/\mathrm{d}x_1 = 0$, in which case the solution can be obtained by solving the quasi-parallel eigenvalue problem of the classical linear stability theory (LST). Equation (2) is to be solved subject to the constraint (imposing the condition that the shape function varies slowly with x_1)

$$F(\alpha, \hat{\phi}) = 0 \tag{4}$$

The functional $F(\alpha, \hat{\phi}) = 0$ can be chosen in several ways. For example, we can impose the condition that the maximum of the velocity component $\hat{u}_1$ is constant (that is, $\partial \hat{u}_1/\partial x_1 = 0$ at the location in the boundary layer where $\hat{u}_1$ is maximum) or the integral constraint[27] that

$$\int_0^\infty q^\dagger \frac{\partial q}{\partial x_1}\,\mathrm{d}x_3 \Big/ \int_0^\infty |q|^2\,\mathrm{d}x_3 = 0 \tag{5}$$

where $q = (\hat{u}_1, \hat{u}_2, \hat{u}_3)$ and the dagger superscript represents the complex conjugate. An iterative procedure for α based on Eq. (5) is given as follows:

$$\alpha_{n+1} = \alpha_n - i\left[\left(\int_0^\infty q_n^\dagger \frac{\partial q_n}{\partial x_1}\,\mathrm{d}x_3\right) \Big/ \left(\int_0^\infty |q_n|^2\,\mathrm{d}x_3\right)\right] \tag{6}$$

where subscript n indicates iteration level. We note that Eq. (6) represents a two-dimensional iterative map whose convergence is by no means guaranteed. However, experience with various incompressible and compressible flows have shown that it provides a satisfactory approach for computing α.

Thus, the procedure to solve PSE consists of solving Eq. (2) numerically by marching from the initial station at $x_1 = (x_1)_0$ with some initial condition, $\hat{\phi}[(x_1)_0, x_3]$. In the present analysis, the initial condition is provided by solving the eigenvalue problem associated with a localized version of PSE. The solution at $x_1 = (x_1)_0 + \delta x_1$ is computed with $\alpha[(x_1)_0 + \delta x_1] = \alpha[(x_1)_0]$ as a first approximation. Then a new α is calculated using Eq. (6). Equation (2) is solved again with the new value of α. This process continues until the solution converges. The marching is then carried to the next x_1 station.

This marching procedure is ill-posed, and the solution will eventually blow up for a sufficiently small marching step size. However, a stable marching solution can be obtained by modifying the pressure gradient term in the marching direction or by taking sufficiently large marching steps. (See Li and Malik.[28,29]) We use the method of Ref. 30 for the numerical solution of the governing equations, that is, Eq. (2). The disturbance growth rate can be computed by defining disturbance kinetic energy as

$$E = \int_0^\infty \bar{\rho}\left(|\hat{u}_1|^2 + |\hat{u}_2|^2 + |\hat{u}_3|^2\right)\mathrm{d}x_3 \tag{7a}$$

with

$$\sigma_E = -\mathrm{Im}(\alpha) + \frac{0.5}{E}\frac{\mathrm{d}E}{\mathrm{d}x_1} \tag{7b}$$

For LST analysis, the disturbance growth rate simplifies to

$$\sigma = -\mathrm{Im}(\alpha) \tag{8}$$

Mean Flow Computation

The computational fluid dynamics (CFD) code used in this study to obtain the mean flow is the GASP code,[31] which has many features that make it suitable for the present work. It solves the steady and unsteady Navier–Stokes equations and its subsets, such as the thin–layer Navier–Stokes (TLNS) equations, the parabolized Navier–Stokes (PNS) equations, and the Euler equations. It models finite rate, equilibrium, and frozen chemistry. It also has equilibrium and nonequilibrium thermodynamics models, as well as a variety of models for viscosity, thermal conductivity, thermodynamics, and diffusion. These features make it easy to ensure that the solution is compatible with the RFPSE.

The version of GASP code used here is written for structured grids using a multiblock, cell-centered, finite volume formulation. The solution scheme is upwind-biased with characteristic-based flux differencing developed by Roe and Van Leer, making it a robust solver. The code also has a variety of explicit and implicit time-integration schemes and convergence acceleration techniques. It has a wide array of boundary condition types covering practically all types of flows. It is also possible to specify pointwise varying values at selected boundaries. At the time this study was made, the available version of the code had only the fully catalytic or noncatalytic option.

The code GASP has a number of chemistry models that can be invoked in the frozen, equilibrium, or finite rate mode. Note that equilibrium flow is modeled by setting the reaction rates to a very large (infinite) value. This technique, thus, drives the solution to an equilibrium composition by artificially decreasing the reaction times relative to the flow residence time. However, within RFPSE, equilibrium composition is computed for a given temperature and pressure based on free-energy minimization. Even though the techniques are different, the two approaches should be compatible because the end result of equilibrium composition is the same.

Chemistry, Thermodynamics, and Transport Properties

The RFPSE code requires the availability of mean flow profiles computed by taking account of the high-temperature effects. In principle, these profiles can be provided by any CFD code, although, in the present study, we selected the GASP code to compute the mean flow. The RFPSE code also requires terms involving μ (viscosity), C_p (specific heat), k (thermal conductivity), h (enthalpy), ρ (density), and P (pressure), as well as species concentrations. Also needed are their derivatives and chemical source terms. Output of all of these quantities from the mean flow code would require a very large data file, which will then need to be interpolated to the RFPSE computational grid. Therefore, the practice we adopt is that only the necessary profiles from the CFD code are stored in a file and the required properties and derivatives are computed within the RFPSE code. The chemistry, thermodynamics, and transport properties (CTTP) program segment is incorporated in the RFPSE stability analysis program to model high-temperature effects.

The modeling is restricted to air chemistry. Furthermore, it is assumed that there is no surface ablation with associated moving boundaries and phase changes. Mass transfer at the surface (blowing or suction) is also not considered. As mentioned before, we only consider the case of thermal equilibrium. It is also assumed that, for the case of flows with chemical nonequilibrium, surface catalysis is implemented in the mean flow code to obtain the correct species profiles near the wall. (Hence, no special treatment is required in the CTTP model.)

The input mean flow formats are of two types, one for the perfect gas and equilibrium gas case in which the velocity vector, $\bar{T}$, and $\bar{p}$ profiles are read in. The second format is suitable for the finite rate chemistry case in which the velocity vector, $\bar{T}$, $\bar{\rho}$, and the species composition profiles $\bar{c}_i$ are input. The equilibrium case can be run in two ways. In the first case (Fig. 1), the species composition is computed by a free-energy minimization method[32] within the CTTP model. The second case permits the computation of stability characteristics under chemical equilibrium from a restart file. The restart option is provided for repetitive stability runs for a given mean flow; this avoids repetitive, and relatively expensive, computation of equilibrium composition and property derivatives.

The number of species used in the CTTP model depends on a parameter kmodel; values of kmodel {1, 2, 3, 4} correspond to number of species {5, 7, 9, 11}. The species order used in CTTP and RFPSE is N_2, O_2, N, O, NO, NO^+, e^-, N^+, O^+, N_2^+, O_2^+. Depending on kmodel, a maximum of 20 reactions[33] are considered. Similarly, a number of options are provided in CTTP for viscosity, thermal conductivity, and other properties. However, we describe here only those relevant to the present application described in the next section.

In the present study, we have used a five-species model (N_2, O_2, N, O, NO) with eight reactants (including three catalytic bodies M_1, M_2, and M_3) and the following reactions ($N_r = 6$):

$$\begin{aligned} &\mathrm{O_2} + M_1 \rightleftharpoons 2\mathrm{O} + M_1, \qquad &&\mathrm{N_2} + M_2 \rightleftharpoons 2\mathrm{N} + M_2 \\ &\mathrm{N_2} + \mathrm{N} \rightleftharpoons 2\mathrm{N} + \mathrm{N}, \qquad &&\mathrm{NO} + M_3 \rightleftharpoons \mathrm{N} + \mathrm{O} + M_3 \\ &\mathrm{NO} + \mathrm{O} \rightleftharpoons \mathrm{O_2} + \mathrm{N}, \qquad &&\mathrm{N_2} + \mathrm{O} \rightleftharpoons \mathrm{NO} + \mathrm{N} \end{aligned} \tag{9}$$

The preceding chemistry model has been used by many researchers to model reacting flows at hypersonic conditions (for example, Gupta et al.,[33] Blottner et al.,[34] and Prabhu et al.[35]).

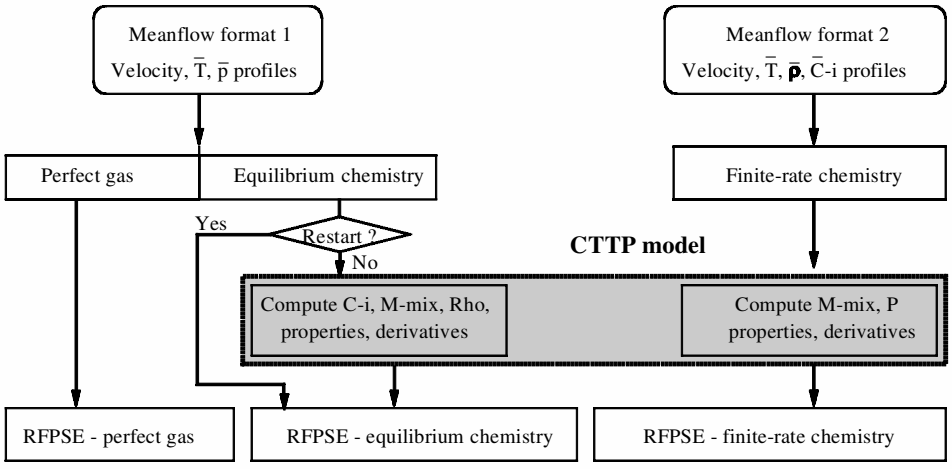

Fig. 1 Program flowchart illustrating mean flow formats, CTTP model, and RFPSE; *C-i* represents the species mass fraction, and *M*-mix is the mixture molecular weight.

We use Wilke's mixing rate[36] with species viscosities taken from Miner et al.[37] We note that the species viscosity formulation of Ref. 34 is more commonly used in the literature. However, for $T < 400$ K, the mixture viscosity computed by the Blottner et al.[34] is higher than the values given by the Sutherland law, which is known to be accurate at relatively low temperatures. The viscosity option selected here blends the Sutherland law at low temperatures with the Blottner et al.[34] formulation at the higher temperatures, resulting in a uniformly valid viscosity formulation for a wide range of temperatures. This viscosity formulation was not available in the original GASP code and was implemented by us to provide compatibility between the GASP mean flow and RFPSE stability analysis.

For thermal conductivity, we use Eucken's relation (see Ref. 38; also used in Ref. 34) in conjunction with Wilke's[36] mixing rule. Multicomponent diffusion is considered where the coefficients of diffusion are taken from Ref. 34 (see also Ref. 33). The thermodynamic properties are calculated using the "Lewis Research Center curve fits," which are also included in the GASP code. Thus, the thermodynamic properties incorporated in CTTP are consistent with those used in the mean flow solver.

Results and Discussion

Mach 6 Sharp Cone

We first consider a relatively low-Mach-number hypersonic case, for which boundary-layer theory with the perfect gas assumption is applicable and, therefore, could provide a check on the quality of mean flow profiles generated by using the Navier–Stokes solver. The geometry considered here is a 5-deg half-angle, 18-in.-long, sharp cone. The freestream conditions are $M_\infty = 6$, $T_0 = 810^\circ$R (450 K), $P_0 = 14{,}400$ psf (6.89×10^3 N/m^2) [$P_\infty = 9.12$ psf (4.37×10^2 N/m^2), $T_\infty = 98.78^\circ$R (54.88 K), $\rho_\infty = 5.382 \times 10^{-5}$ slugs/ft^3 (2.77×10^{-2}kg/m^3), and $Re_\infty = 2.1 \times 10^6$/ft ($6.9 \times 10^6$/m)]. The wall is assumed to be adiabatic, and the theoretical postshock conditions for boundary-layer calculation are $M_e = 5.5852$, $P_0 = 14{,}380$ psf (6.89×10^5 N/m^2), $T_e = 111.89^\circ$R (62.16 K), and $P_e = 14.09$ psf (6.74×10^2 N/m^2).

The numerical grid used for the GASP code is shown in Fig. 2. The grid was generated algebraically as a trapezoidal pie-shaped region of two planes in the circumferential direction and with orthogonality at the wall. The wall-normal grid consists of 81 equispaced points within an estimated boundary-layer thickness variation. An additional 80 points are stretched out to the outer computational boundary. In the streamwise direction, the spacing is 0.25 in. near the cone base with clustering near the apex.

The mean flow solution with the perfect gas assumption was obtained by the use of the GASP code and by the use of the boundary-layer code of Harris and Blanchard.[39] The Navier–Stokes solutions are based on Roe's flux-difference splitting and with "min-mod" limiters to handle the shock, while keeping third-order accuracy away from the shock. The interface procedure for this case is relatively simple because the grid is two-dimensional and orthogonal to the surface.

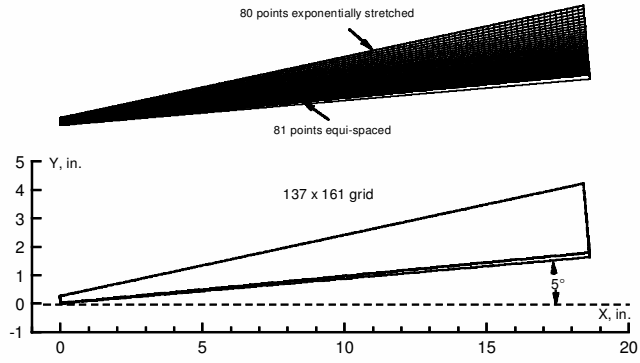

Fig. 2 Navier–Stokes grid employed for the Mach 6 cone flow; *x* is the axial distance.

Figure 3 compares the boundary-layer(BL) code solution with the GASP solution at the four surface locations indicated. The streamwise and normal velocities, as well as temperature and density profiles, are shown. The normal grid resolution appears to be adequate for stability analysis. Comparison is good for the velocity and the temperature profiles; however, the density profiles are off slightly. The boundary-layer edge value of the density from the GASP solution is higher, especially at locations close to the apex.

Figure 4 shows a plot of the surface pressure variation from the GASP solution as compared with the theoretical postshock value and an inviscid GASP computation on an Euler grid. It is clear that the shock/boundary-layer interaction sets up a streamwise pressure gradient that is responsible for the difference in the density profiles. To confirm this, a boundary-layer code solution was obtained by the use of the GASP surface pressure distribution. Comparison of the resulting boundary-layer profiles with the GASP profiles is shown in Fig. 5. Note that all of the profiles are now in much better agreement. Computations were also performed by the use of the CFL3D code,[40] which gave very similar results. It has been our experience that, given a suitable grid, the CFL3D code can provide reasonably accurate mean flow profiles for stability analysis. (See also Ref. 41.) However, we require a CFD code with chemistry effects for the present study and only the perfect gas option is incorporated in CFL3D.

This comparison of mean flows served to bring out the following key points: 1) The shock/boundary-layer interaction effect in high Mach number is noticeable even for the sharp slender bodies. 2) These effects are at least partially accounted for in a boundary-layer calculation by imposing the "true" surface pressure variation. 3) A TLNS or, at least, a PNS calculation is requried for computing mean flow profiles.

Stability computations were performed using various mean flows computed here. The four different mean flows used are

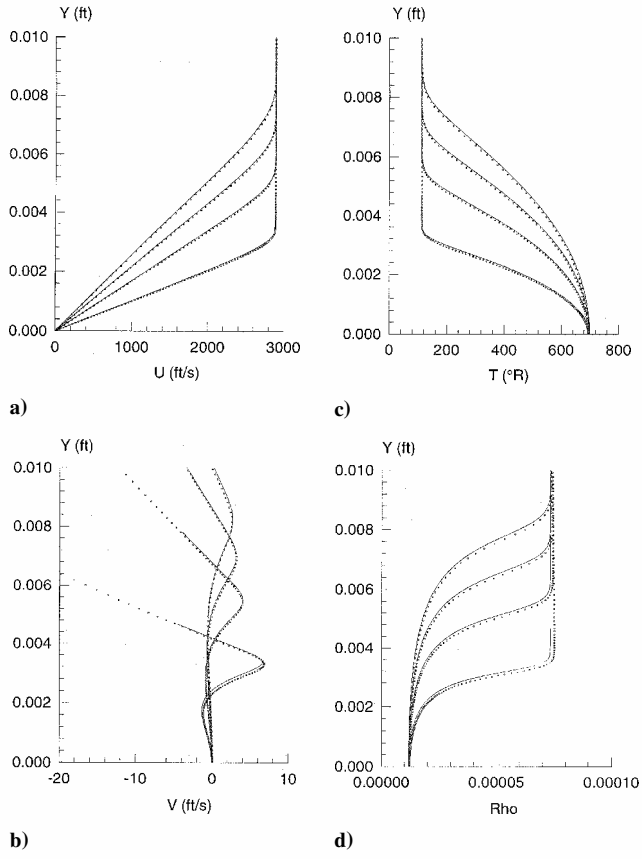

Fig. 3 Comparison of mean flow profiles for Mach 6 cone flow at x = 0.25, 0.67, 1.08, and 1.50 ft: ——, BL and · · · ·, GASP.

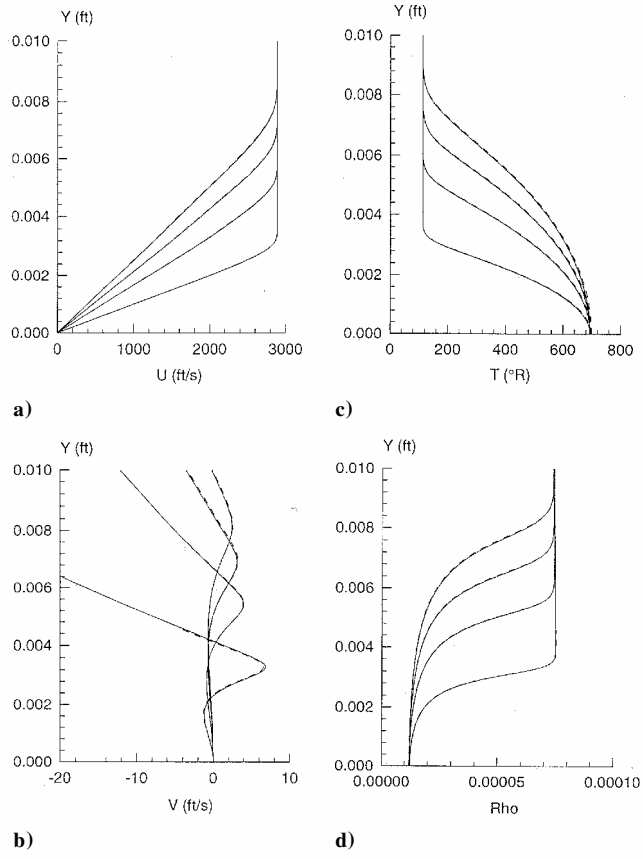

Fig. 5 Comparison of mean flow profiles for Mach 6 cone flow at x = 0.25, 0.67, 1.08, and 1.5 ft: ——, GASP and - - - -, BL (with GASP C_p).

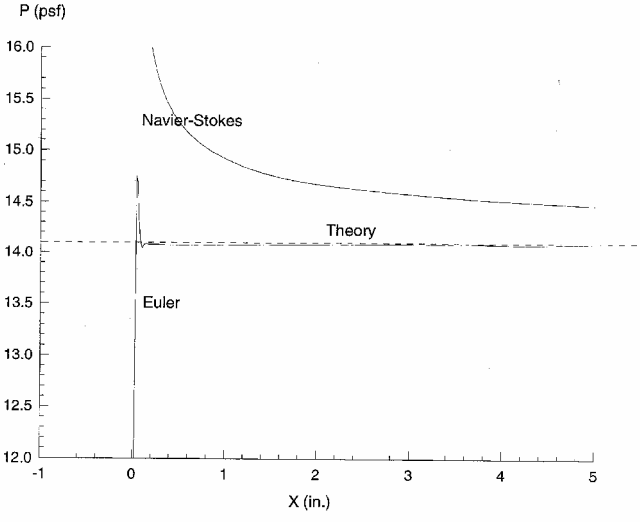

Fig. 4 Surface pressure variation for Mach 6 cone flow.

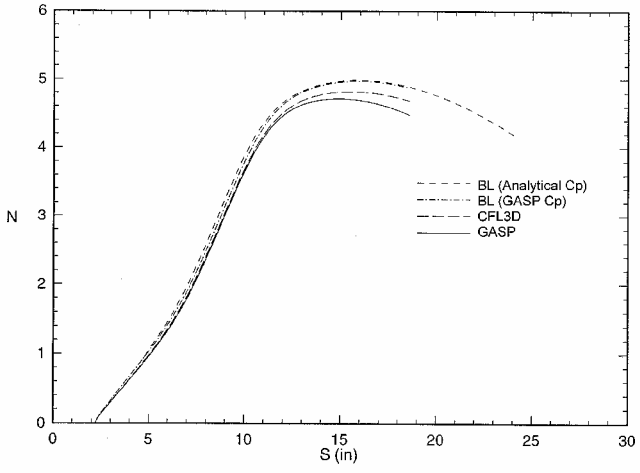

Fig. 6 Comparison of nonparallel (PSE) N factor for various mean flows.

1) a boundary-layer solution with an analytical (that is, constant) wall-pressure condition, 2) a boundary-layer solution with GASP surface pressure distribution, 3) a CFL3D TLNS solution, and 4) a GASP PNS solution. Growth rates and N-factor results were obtained using quasi-parallel theory and PSE for a disturbance with a frequency of 200 kHz. The results can be summarized by presenting the PSE N-factor variation as shown in Fig. 6. Results based on CFL3D and GASP codes are initially the same, but they diverge toward the end of the computation, with a maximum difference in N factor of about 0.2. N factors based on the two boundary-layer solutions are generally quiet close, and they both are somewhat higher than those based on the CFD codes. The maximum difference in N factor using a boundary-layer solution and CFL3D is about 0.2. If we consider the N-factor results obtained using the CFL3D mean flow to be the most physically correct, the estimated error in both GASP–PNS and boundary-layer based N factors is about 4%.

Reentry-F Cone

We now present results of our computations for the Reentry F cone, for which flight transition data are available. The Reentry-F flight vehicle[22,23] consisted of a 5-deg semivertex cone with a nominal nose radius of 2.54×10^{-3} m. Reentry-F flight data have been analyzed by Zoby and Rumsey,[42] Thompson et al.,[43] and Wurster et al.[44] In these studies, various engineering codes and viscous shock layer equations were used to compute laminar and turbulent flow with transition onset locations specified via a correlation of the Reentry-F experimental data. Overall, good agreement with the experimental heat flux distributions were obtained. The objective of

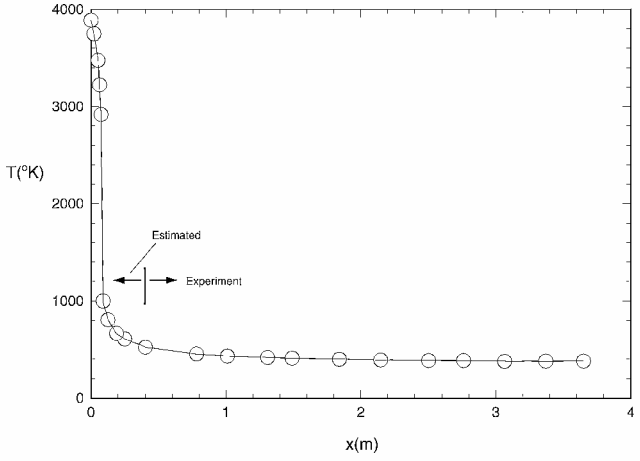

Fig. 7 Wall temperature distribution used for Reentry-F cone calculation.

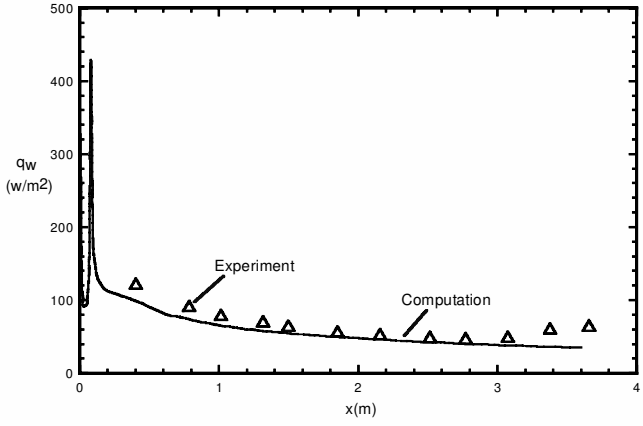

Fig. 8 Comparison of computed and measured wall heat flux.[20]

the present study is to analyze laminar boundary layer for its stability and to evaluate the applicability of the e^N method. Therefore, we need a case where a substantial run of laminar flow was present with transition onset somewhere on the cone. To avoid roughness induced by nose ablation, it is desirable to have a case for which the nominal nose shape is maintained. Therefore, we perform computations for an altitude of 30.48 km (100,000 ft) where the nose radius was estimated to increase only slightly due to ablation, that is, 3.1×10^{-3} m (0.0102 ft). The freestream Mach number was 19.925 and the freestream temperature was 228 K (408.6°R). The associated freestream Reynolds number was 6.56×10^6/m (2×10^6/ft). The nose of the vehicle back to 0.22 m was constructed from ATJ graphite, whereas the rest of the vehicle was made of beryllium. A physical discontinuity at the graphite–beryllium junction was present, but the experimental information about wall temperature in this region is not available.

The particular case selected here for analysis was studied earlier by Malik et al.[20] For mean flow computations, they used the equilibrium gas Navier–Stokes code of Gnoffo[45] for the nose region and a PNS code, UPNS (Tannehill et al.[46]), for the downstream region. The wall temperature distribution used in Ref. 20 is given in Fig. 7. Wall temperatures in the region $x \geq 0.4$ m were taken from the experimental measurements[47] and the temperature in the region $x < 0.4$ m were computed estimates provided by E. V. Zoby of NASA Langley Research Center (private communication, 1988). The physical discontinuity (step/gap) referred to was ignored in the analysis of Ref. 20, as well as here. Figure 8 shows a comparison of the wall heat flux computed in Ref. 20 with the available experimental data. Reasonable agreement with the experiment was found in the region where experimental data were available. The reason for the sharp peak in the computed heat flux distribution was not fully investigated. The rise in the experimental heat flux around $x = 2.9$ m

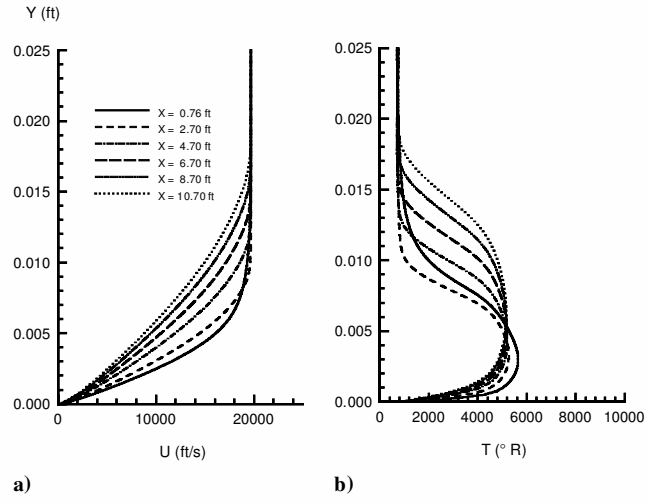

Fig. 9 Velocity and temperature profiles for the Reentry-F cone using equilibrium gas assumption.

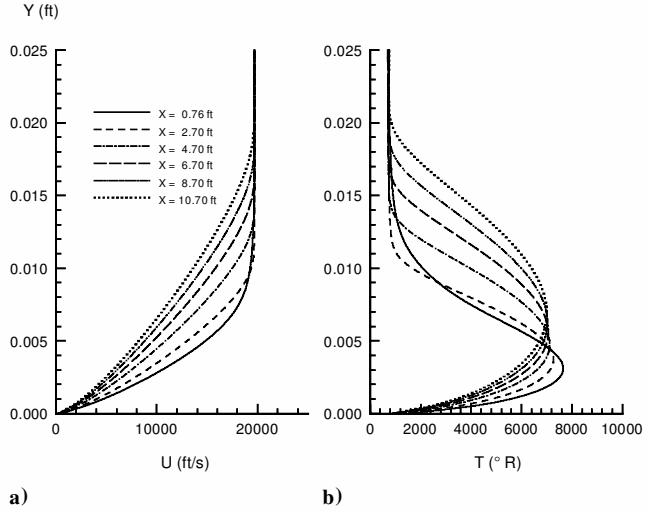

Fig. 10 Velocity and temperature profiles for the Reentry-F cone using finite rate chemistry.

(9.5 ft) is an indication of the beginning of transition. In view of the comparison of the computed and experimental heat flux variation in the laminar region shown in Fig. 8, the comment in Ref. 25 that "the mean heating in the Malik et al. computations appeared high" is without justification.

The wall temperature distribution of Fig. 7 was also adopted for the present computations. The grid for this case consists of two zones. The first zone covers the nose region, as well as part of the cone up to 0.04 ft (49×161 grid). Computation in this region is done by using the TLNS version of GASP. The second zone is completely on the straight portion of the cone and employs a 141×161 grid. Computation in this zone is done using the PNS option of GASP, with inflow conditions specified by the converged solution from zone 1. Again, 81 of the 161 wall-normal points are uniformly spaced in an estimated boundary-layer thickness, whereas the rest are stretched out to reach the outer computational boundary.

Meanflow computations were performed using perfect gas, equilibrium gas, and finite rate chemistry options. Figures 9 and 10 show the streamwise velocity profiles and temperature profiles at six stations on the straight part of the Reentry-F cone under chemical equilibrium and nonequilibrium conditions, respectively. The peak temperatures for the nonequilibrium flow are significantly higher compared to the equilibrium case. As a result, the boundary layer is also thicker. The species concentration profiles from the two computations are also different, as shown in Figs. 11 and 12, where the

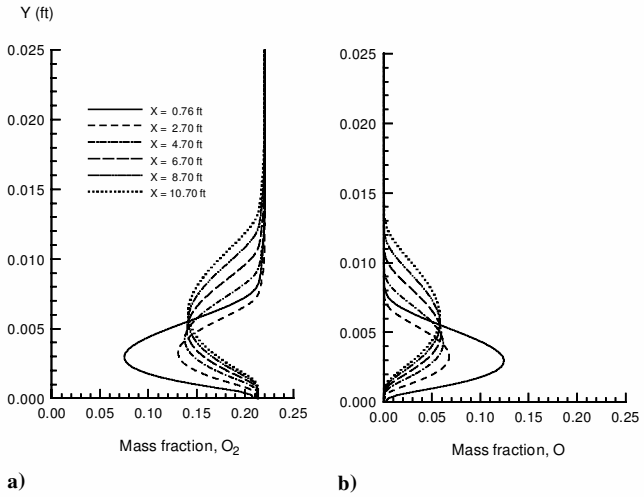

Fig. 11 Concentration profiles for O_2 and O for the Reentry-F case using equilibrium gas assumption.

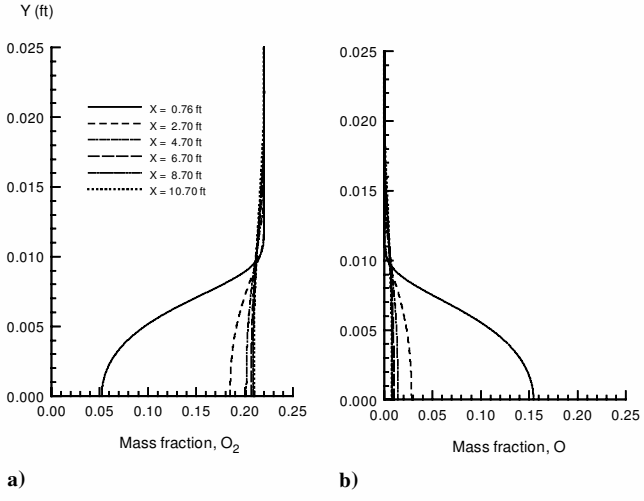

Fig. 12 Concentration profiles for O_2 and O for the Reentry-F case using finite rate chemistry and noncatalytic wall.

mass fraction profiles of O_2 and O are presented for equilibrium and nonequilibrium conditions, respectively. The main reason for this difference can be attributed to the wall boundary conditions for the species equations. For equilibrium calculations, the species concentrations at the wall are determined by the equilibrium distribution corresponding to the prescribed wall temperature. However, for the finite rate chemistry case, the wall is assumed to be noncatalytic, yielding a zero normal concentration gradient at the wall. The effect of a catalytic, or partially catalytic, wall on finite rate chemistry results was not studied. As noted earlier, these results were obtained with the five-species chemistry model. Calculations with larger numbers of species were also performed, but did not show any appreciable change in the mean flow profiles because the newly added species exist only in minute amounts.

We now present results for the stability analysis of the Reentry-F mean flow. Here, we first consider the equilibrium gas assumption and quasi-parallel approximation because the results of Ref. 20 were also obtained under these restrictions. N-factor results for axisymmetric disturbances of various frequencies (ranging from 200 to 480 kHz) are presented in Fig. 13. As noted, the beginning of transition in the flight experiment was estimated to be at $x = 2.9$ m, which yields a Reynolds number based on freestream conditions of about 1.9×10^7. The value of the N factor at this location is 7.9, and the corresponding disturbance frequency is 240 kHz. These values of N factor and disturbance frequency are to be contrasted with the values of 7.5 and 240 kHz, respectively, computed in Ref. 20. In Ref. 20, the shock-fitting Navier–Stokes

Table 1 N-factor results (at $x = 2.9$ m) for Reentry-F cone using different options of the RFPSE code

Option	Perfect gas	Equilibrium gas	Finite rate chemistry
Quasi-parallel	6.5	7.9	8.1
Nonparallel	7.3	9.8	9.5

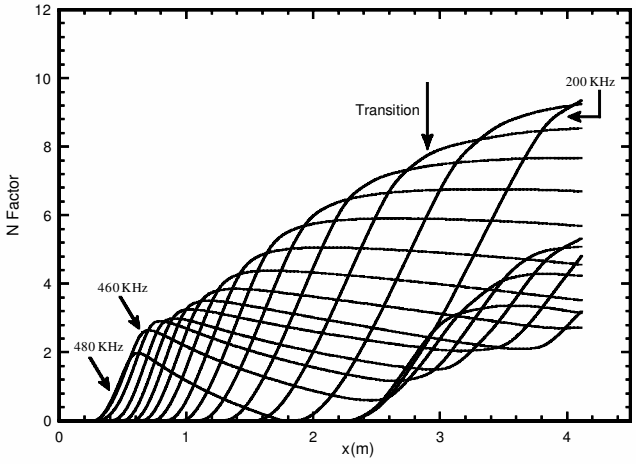

Fig. 13 N factor results for the Reentry-F cone using quasi-parallel (LST) and equilibrium gas options of RFPSE. Disturbance frequencies vary from 200 to 480 kHz.

code of Gnoffo[45] was employed for the nose region, followed by the UPNS code of Tannehil et al.[46] that was used to march the solution up to $x = 3.65$ m. The UPNS code was used in several steps with successively increasing the streamwise grid size. Because the code is noniterative, a total of 80,000 grid points were used in the x direction with a total of 240 grid points in the cross-stream direction. On the other hand, the present solution was obtained by using GASP-TLNS in the nose region, followed by GASP-PNS on the straight cone. In the GASP-PNS computation, we used 161 points in the wall-normal direction and only 141 points in the x direction. A relatively small number of points in the x direction can be afforded because GASP-PNS employs an iterative marching algorithm. Given that the two computations were performed almost a decade apart using two different suites of CFD and stability codes, agreement between the two sets of results is very good.

Analysis of the eigenfunctions and the range of values of the disturbance phase velocity shows that the disturbances that amplify in the Reentry-F cone boundary layer are the second mode[4] disturbances. Note in Fig. 13 that high-frequency disturbances (that is, 460 kHz) amplify, decay, and then amplify again. The second region of growth is associated with the third mode of instability, also found in Ref. 20. However, the third mode N factors are lower than those for the second mode.

N-factor results using PSE are presented in Fig. 14 for the equilibrium gas assumption and in Fig. 15 for the finite rate chemistry option. Note that the PSE computations account for mean flow variations (nonparallel effect) and transverse curvature. N factors at the location of transition are found to be 9.8 and 9.5, respectively. Other calculations using a perfect gas with a quasi-parallel approximation LST were also performed. Table 1 contains a summary of all of the results. The comparison shows that nonparallel effect is destabilizing for all three gas models selected. The effect of gas chemistry is also destabilizing, although it does not matter much whether one considers the assumption of chemical equilibrium or finite rate chemistry. As an example, let us assume that $N = 10$ (based on PSE) is taken as an indicator for the onset of transition. Then, the equilibrium and finite rate chemistry calculations would yield transition onset locations to be 3 and 3.13 m, respectively, whereas the perfect gas PSE calculation (not shown in this paper) would yield transition onset off of the base of the cone at about 4.4 m. The preceding conclusions are reiterated by plotting

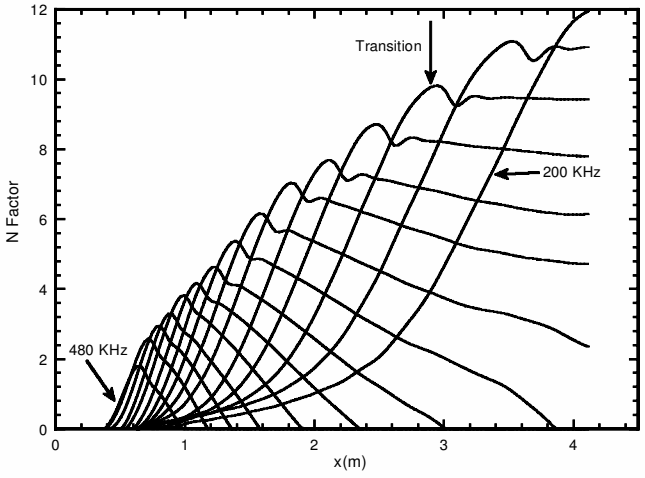

Fig. 14 Same as in Fig. 13, except that nonparallel option of RFPSE code was used.

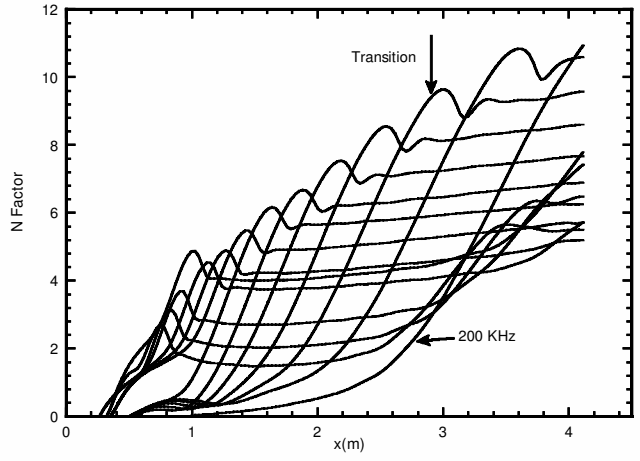

Fig. 15 *N* factor results using RFPSE and finite rate chemistry for disturbance frequencies of 200–460 kHz.

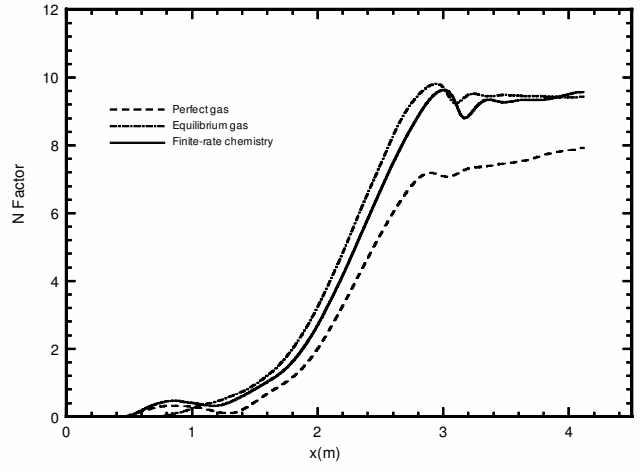

Fig. 16 Comparison of perfect gas, equilibrium gas, and finite rate chemistry-based RFPSE (nonparallel) *N* factor for f = 240 kHz.

the N-factor results for the disturbance frequency of 240 kHz in Fig. 16. Using equilibrium gas model, Malik and Anderson[16] had earlier concluded that the effect of chemistry is to destabilize second mode disturbances. Using the quasi-parallel reacting flow theory of Ref. 19, Johnson et al.[48] found that the inclusion of air chemistry destabilized the cone boundary layer for the shock tunnel experiments of Germain and Hornung,[49] in comparison with the perfect gas assumption.

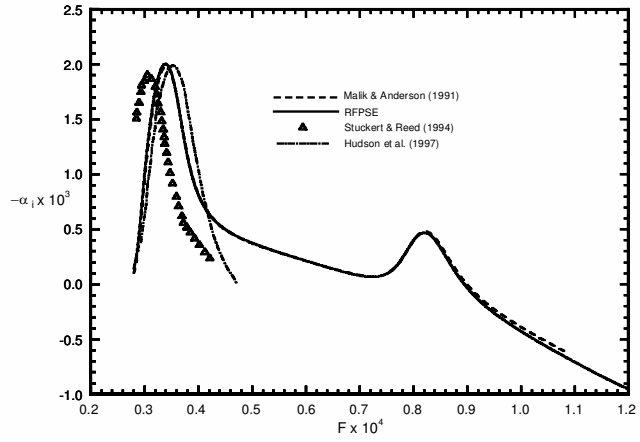

Fig. 17 Comparison of the RFPSE disturbance growth rates (using quasi-parallel assumption) with results of previous investigations for the Mach 10 flat-plate boundary layer (R = 2000, real gas in equilibrium).

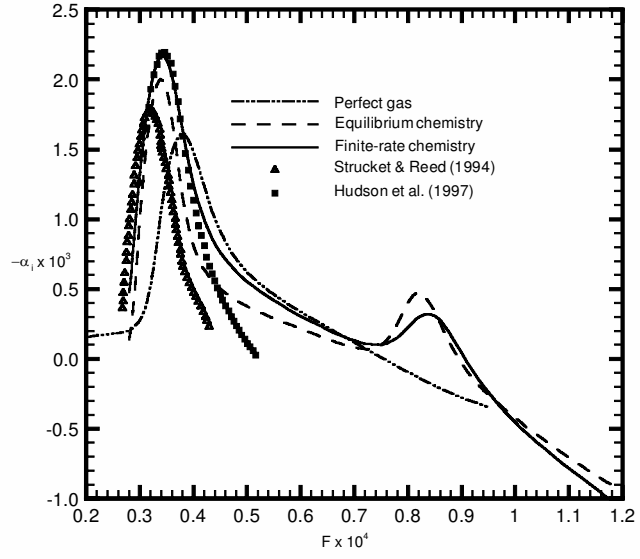

Fig. 18 Quasi-parallel growth rate of two-dimensional disturbances for three gas models using RFPSE (Mach 10 flat-plate boundary layer, R = 2000); finite rate chemistry results from Refs. 18 and 19 are also shown.

This conclusion related to an equilibrium vs nonequilibrium assumption is not a general conclusion and has to be considered specific to the conditions of Reentry-F cone experiment. For Mach 20 flow past a 6-deg wedge, Chang et al.[50] computed N factors using RFPSE and by selecting perfect gas, equilibrium gas, and finite rate chemistry models. It was found that $N = 10$ would predict transition onset location to be at 39, 24, and 14 ft, respectively, from the leading edge, for these gas models. The marked difference between the three results was attributed to the effect of chemistry on the supersonic instability mode,[5] which was destabilized significantly in the case with the equilibrium gas assumption. We note that, using the quasi-parallel option of RFPSE with the equilibrium gas assumption, Chang et al.[50] also computed stability results for the Mach 10 adiabatic wall test case of Ref. 16. Their results, along with those of Refs. 16, 18, and 19, are given in Fig. 17. It can be seen that RFPSE results using the equilibrium gas assumption agree well with the results of Ref. 16, hence providing mutual validation of the codes. The effects of gas chemistry (finite rate, equilibrium, and perfect gas) on the stability of the Mach 10 flat-plate boundary layer is shown in Fig. 18, using the quasi-parallel version of RFPSE. As first found in Ref. 15, the real gas effect shifts the most unstable second mode disturbance to lower frequencies. The growth rate with finite rate chemistry are somewhat higher than the case with the equilibrium

gas assumption. The finite rate chemistry results of Stuckert and Reed[18] and Hudson et al.[19] are also shown. Overall, the RFPSE results are closer to the results of Ref. 19 than those of Ref. 18, both for equilibrium gas and nonequilibrium gas. The difference in stability results is likely caused by different mean flow solvers: Refs. 16 and 50 used boundary-layer codes, whereas Refs. 18 and 19 employed PNS solvers.

For the Reentry-F cone, the N factor value of 8.1 using the quasi-parallel finite rate chemistry option of RFPSE is to be contrasted with the N factor value of about 5.5 (Malik et al.[51]) obtained by using a perfect gas assumption for the Stetson et al. Mach 8 sharp cone experiment[8] and the values in the range of 3.1 and 6.6 obtained by Johnson et al.[48] for the shock tunnel experiments of Ref. 49 using air. Tunnel noise is expected to be the main contributing factor between the N values of Refs. 48 and 51 and that of the Reentry-F cone.

Sherman–Nakamura Reentry Experiment

We will now attempt to simulate the flight transition experiment described by Sherman and Nakamura,[24] hereafter referred to as S–N. As noted by Schneider,[52] not all of the necessary details of this experiment are available, which forced us to make several assumptions to compute the mean flow. What is known is that the experiment was performed on a 22-deg half-angle blunt cone with beryllium skin and graphite nosetip, but the nose radius is not given. Figure 4 of S–N indicates that, at an altitude of 110,000 ft, transition onset coincided with the second set of sensors on the cone. These sensors were located at $s/r_n = 91.6$, where r_n is the nose radius and s is the surface distance. (See Fig. 1 of Ref. 24.) Based on data presented by Berkowitz et al.,[53] Schneider[52] inferred that the nose radius was about 0.25 in. With this value, the location of transition onset is about 23 in. downstream of the nose. Figure 4 of S–N shows that the surface temperature at the transition onset location was about 800°F. Therefore, except very near the nose, we assume the wall temperature to be about 1300°R. We chose a Mach number of 22, which yielded a freestream velocity of 22,141 ft/s at the altitude of 110,000 ft. This value of freestream velocity is in reasonable agreement with the value of 22,310 ft/s listed under data point 74 of Berkowitz et al.,[53] which, according to Ref. 52, is taken from Ref. 24. For this data point, Berkowitz et al. list $S_{\text{tr}} = 24.3$ in., $T_w = 1309$°R, $P_e = 1437$ psf, $M_e = 6.25$, and $Re_s = 3.75 \times 10^6$ (S–N report $M_e = 6.2$ for 110,000-ft altitude). Thus, the wall temperature value and the transition onset locations are in reasonable agreement with our assumed values. The freestream conditions at the selected altitude are $T_0 = 40966.4$°R, $P_0 = 139{,}401$ kpsf ($P_\infty = 14.9557$ psf, $T_\infty = 419.27$°R, and $\rho_\infty = 2.0666 \times 10^{-5}$ slug/ft^3). The associated freestream Reynolds number is 1.44421×10^6/ft, giving a transition Reynolds number based on freestream conditions of about 2.8×10^6.

As noted, the geometry is a 22-deg half-angle, semi-infinite blunt cone with circular cross section and a nose radius of 0.25 in. Although the cone was spinning, the spin rate was very small compared to the axial velocity, and the angle of attack was assumed to be small. Therefore, the flow is taken to be axisymmetric. The freestream Mach number is 22, which is comparable to the Reentry-F case. However, due to the larger cone angle, flow compression is much more severe, which yields a boundary-layer edge Mach number of about 6 as compared to about 14 computed for the Reentry-F case.

The computational grid used for the GASP code was generated algebraically as a pie-shaped region of two planes in the circumferential direction. An equispaced distribution of 121 points was used within an estimated boundary-layer thickness variation. In the outer region, an additional 120 points are placed, which are stretched out to reach the outer computational boundary. In the first zone, which extends up to $x = 2.5$ in., the TLNS version of the GASP code employing 121 streamwise grid points was used. In the second zone, $2.5 < x \leq 23.5$ in., the PNS version of the GASP code was used by employing 320 streamwise grid points. The finite rate chemistry option of the GASP code was utilized.

As noted, wall temperature distribution is not available from the experiment, except for the temperature at the location of onset of transition, measured to be close to 1300°R. We constructed a T_w distribution by assuming that the temperature at the nose is 7200°R, which is close to the value selected for the Reentry-F case. Wall temperature was assumed to drop from 7200 to 1300°R within 1 in. from the nose and remain constant thereafter. The imposed T_w distribution is shown as curve A in Fig. 19. We will discuss the effect of the assumed temperature distribution later.

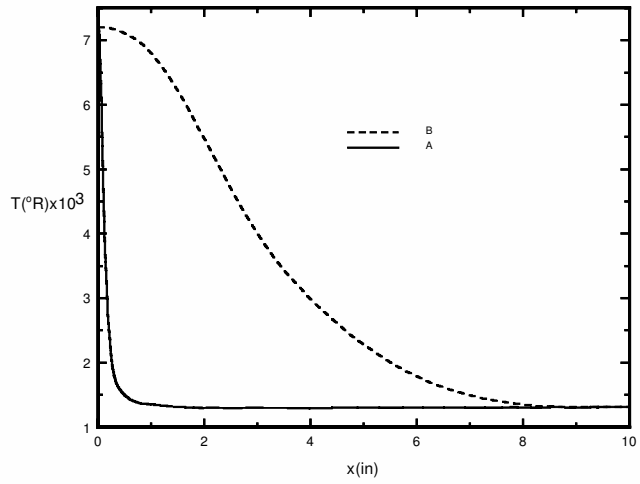

Fig. 19 Assumed wall temperature distributions for the S–N cone experiment.

Figures 20 and 21 show contour plots for pressure and Mach number. Figures 20 and 21 clearly show the bow shock formed ahead of the blunt nose of the cone and that the outer computational boundary is more than twice the shock standoff distance. Close-up examination of pressure and Mach number contours in the stagnation region revealed no evidence of carbuncle instability[54] in the solution. Farther downstream, the shock moves away from the surface and eventually settles at about 70% of the domain height. These results appear to demonstrate that the shock is relatively well resolved; however, we will further comment on this later.

Figure 22 shows wall-normal variation of velocity, temperature, Mach number, and density at some selected x stations. Examination of the Mach number profiles reveal that the Mach number overshoots to a value of about 6.1 before dropping to a value of about 5.6. The boundary-layer edge Mach number at relatively large distances from the nose is 5.6, as compared to the value of 6.2 given by S–N (and 6.25 in Ref. 53). The reason for this discrepancy may be attributed to the approximate inviscid techniques used by these authors to analyze high-temperature (real gas) flows or boundary-layer methods to address entropy layer swallowing. Note that the stream temperature (behind the shock but outside the boundary layer) in the present case is about 5875°R (Fig. 22b) as compared to only about 800°R in the case of the Reentry-F cone (Fig. 10b). Therefore, chemistry effects should be more pronounced in the S–N experiment.

The mean flow profiles were analyzed by the use of the RFPSE code with the finite rate chemistry option. The stability results are presented in Fig. 23 for seven disturbance frequencies in the range from 1.5 to 3 MHz. These are purely axisymmetric disturbances, just as in the Reentry-F case. Transition onset in the experiment was indicated to occur at about $s = 23$ in, corresponding to an N factor of approximately 11.2. The most dangerous disturbance frequencies are noted to be in millions of hertz. These high frequencies are a direct result of the thin boundary layer ($\delta \sim 0.047$ in. at $s = 23$ in.) caused by the large cone angle and relatively low wall temperature. Whether the freestream environment can provide the necessary impetus for such high-frequency disturbances in the boundary layer remains an open question. Bushnell[55] has conjectured that the surface electrostatic field near the blunt nose can provide such high frequencies.

As noted, the freestream Reynolds number at the location of transition is about 2.8×10^6, which is to be contrasted with the transition onset Reynolds number of about 1.9×10^7 in the Reentry-F case.

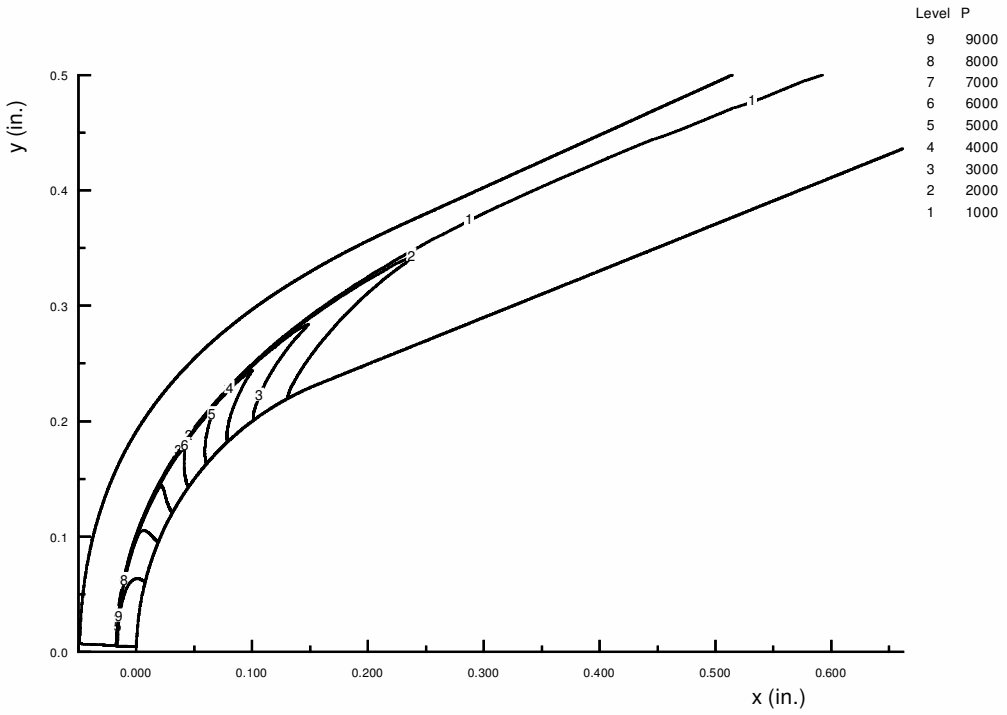

Fig. 20 Computed pressure pounds per square foot contours for the S–N cone.

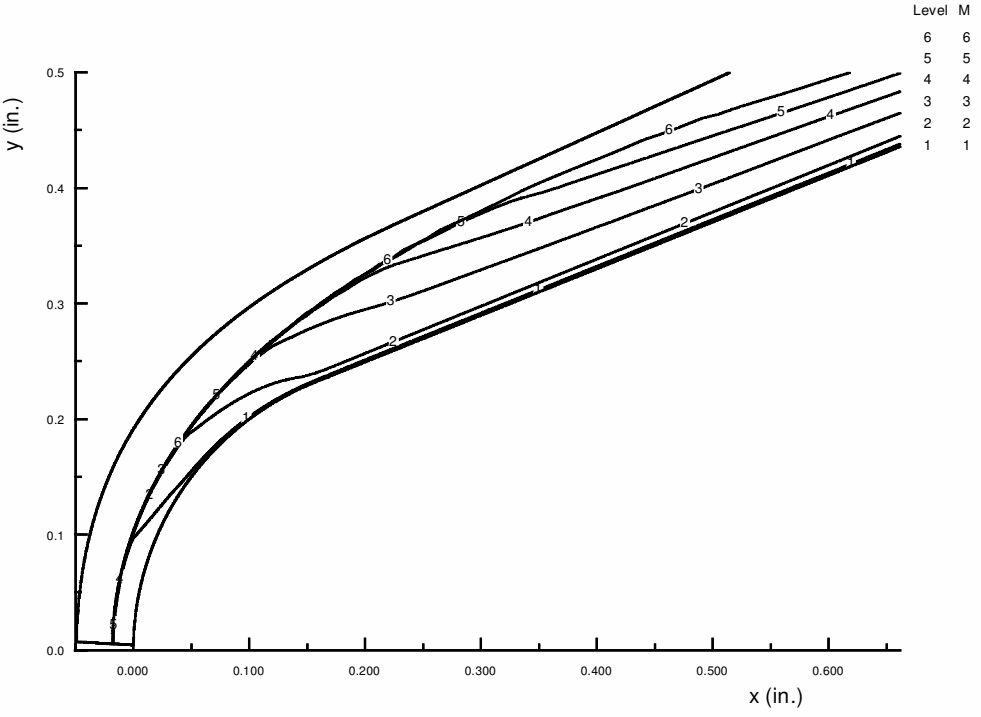

Fig. 21 Computed Mach number contours for the S–N cone.

However, the higher Reynolds number in the latter case may be attributed to the stabilizing effect of Mach number M_e because M_e is only about 5.6 for the S–N experiment, whereas it is about 14 for the Reentry-F case. Both experiments have cold wall conditions (that is, low values of T_w/T_0).

Figure 24 presents the variation in the ratios of disturbance wavelength to boundary-layer thickness (λ/δ) for the seven disturbance frequencies computed by RFPSE. Based on the N-factor results, λ/δ for the most dangerous frequency of 2 MHz at the experimental onset of transition ($s = 23$ in.) is about 2, which correlates well with the expected value for second mode induced transition in hypersonic boundary layers. A certain amount of waviness can be noticed in the λ/δ curves shown in Fig. 24. Similar waviness is also evident in N-factor results given in Fig. 23. The waviness in these results may be attributed to the grid used near the shock, which turned out not to be fully satisfactory because it produced numerical reflections back and forth between the shock and the wall. The effect of these reflections was evident in the wall pressure distribution that influenced boundary-layer thickness variation, which in turn affected disturbance growth rate. An adaptive grid (for example, shock fitting)

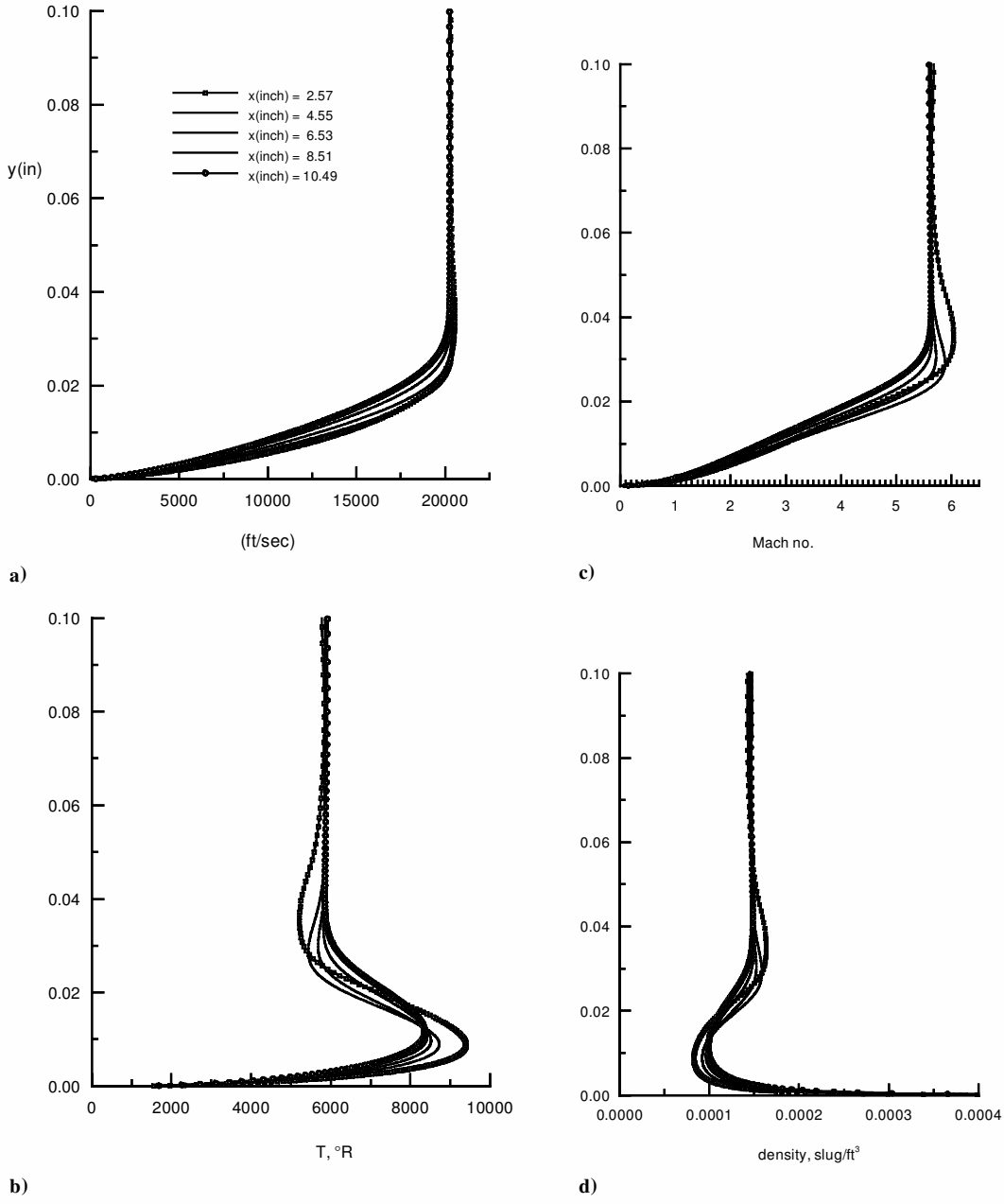

Fig. 22 Mean flow profiles for the S–N cone using finite-rate chemistry.

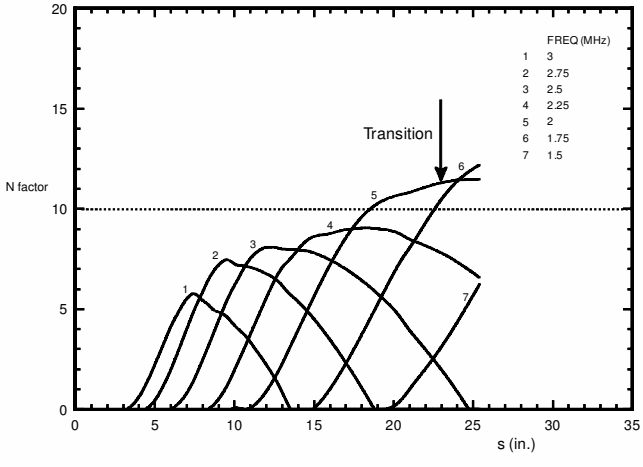

Fig. 23 *N* factors using RFPSE (nonparallel with finite rate chemistry) for the S–N cone.

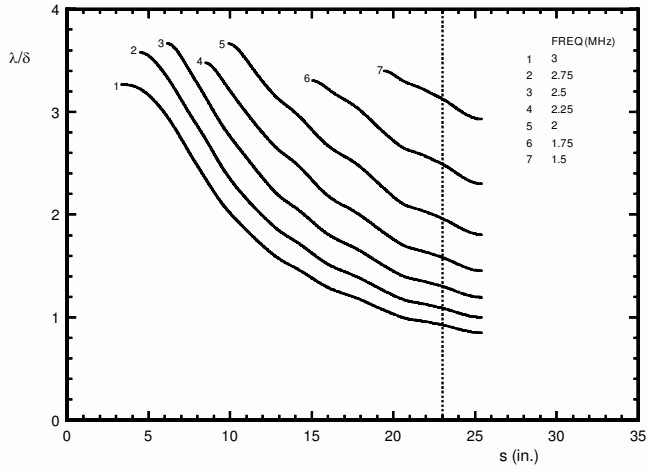

Fig. 24 Ratio of disturbance wavelength to boundary-layer thickness.

would have prevented these reflections from the shock. If such a solution were to be available, our results for the S–N cone will be expected to change. However, we estimate that the N factors presented in Fig. 23 will not change by more than ± 1 and, therefore, our overall conclusions would remain the same.

The results presented in Fig. 23 were obtained by using the temperature distribution A of Fig. 19. As noted, we only know that the wall temperature approaches a value of about 1300°R at large distances from the nose. How it approaches that value was assumed arbitrarily. What effect would a different wall temperature distribution have on the preceding results? To answer this question, we also performed computations by using wall temperature distribution B of Fig. 19, which is an extreme departure from the assumed distribution A. In case B, boundary-layer thickness increased initially (it was 13% higher at $x = 3.6$ in.) but the two thicknesses became almost the same at $x \approx 10$ in. For some relatively high-frequency disturbances (for example, 3 and 2.75 MHz) the maximum growth rate decreased somewhat due to the hotter wall, but the region of growth increased due to the variation in the boundary-layer thickness. This resulted in somewhat higher N factors for these frequencies, but not enough to change the preceding conclusions in any way. N factor results remained essentially unchanged for lower frequencies, in particular, 2 MHz, which became unstable farther downstream. Therefore, it is reasonable to conclude that small uncertainties in wall temperature variation will not affect the location of onset of the transition for this hypersonic experiment.

Finally, we comment on the sensitivity of the stability results to the nose radius and angle of attack of the cone. The effect of nose bluntness on hypersonic boundary-layer transition was studied by Malik et al.[51] for the blunt cone experiment of Stetson et al.,[56] with a nose Reynolds number of 3.125×10^4. It was shown that the effect of this amount of bluntness is significantly stabilizing as compared to a sharp cone boundary layer. The nose Reynolds number for the cone of Ref. 24 is 3.0088×10^4, which is close to the value used in the Stetson et al.[56] wind-tunnel experiment. Because the boundary-layer edge Mach numbers are quite close in the two experiments, it is expected that the effect of nose bluntness will also be similar. However, note that the value of T_w/T_0 is much smaller in the flight experiment, and it is not known whether it will mitigate the effect of bluntness. This question can only be answered by performing additional computations with various combinations of wall temperature and nose radii.

The effect of angle of attack on supersonic boundary-layer transition on a cone has been studied experimentally by King[57] and computationally by Malik and Balakumar.[58] It is known, for example, that an angle of attack of 2 deg has a profound effect on the stability and transition mechanism in the supersonic cone boundary layer studied in Refs. 57 and 59. The empirical parameter that can be used to correlate this effect is the ratio of the angle of attack to the cone angle, which, for the quiet tunnel experiment of Ref. 57, is 0.4 (for an angle of attack of 2 deg). Stetson et al.[59] presented data from various wind-tunnel experiments showing the effect of this parameter on the transition location on the windward and leeward lines of symmetry. According to these data, for a maximum error in transition location of $\pm 10\%$, the value of the parameter (angle of attack/cone angle) should be less than 0.05. Because the cone angle is 22 deg in Ref. 24, a value of 0.05 for this parameter yields an angle of attack of 1.1 deg. Provided the angle of attack for the data point selected for the analysis was less than 1.1 deg, we can expect an error in the transition onset location of $\pm 10\%$. Sherman and Nakamura[24] report little sensitivity of the results to cone angle of attack measured by two rows of sensors, which were 180 deg apart. However, instead of placing these sensors along the windward and leeward lines of symmetry, they were actually located in between the symmetry lines.

Conclusions

In an attempt to analyze high-Mach-number flight transition data, we have computed mean boundary-layer flow using GASP for two high-altitude cases: one from the Reentry-F 5-deg cone experiment[22,23] and the other from the S–N[24] 22-deg cone experiment. Although the freestream Mach numbers were about 20 and 22 for the Reentry-F and S–N experiments, the boundary-layer edge Mach numbers were about 14 and 5.6, respectively, due to the higher cone angle in the latter case. The mean flows were then analyzed by the use of the PSE code with finite rate chemistry effects. For the Reentry-F case, calculations were also performed by the use of perfect gas and equilibrium gas models and by the use of a quasi-parallel approach.

The analysis of the experimental data for these cold wall boundary layers suggest that transition was caused by second mode disturbances in both cases. The disturbance frequencies that correlate the transition onset in the two cases were 240 kHz and 2 MHz, respectively. It was found that the nonparallel effect was destabilizing, as was the chemistry effect. Calculations showed that the estimated transition location (using $N = 10$ as the criterion) in the Reentry-F case would shift from about 3.1 to 4.4 m, if chemistry effects are ignored.

The remarkable thing about the present results is that, in the two test cases, respectively, the local boundary-layer edge Mach numbers are 14 and 5.6, the edge temperatures are 800 and 5875°R, and the Reynolds numbers at the transition onset locations are 1.9×10^7 and 2.8×10^6, yet the N factors at the experimentally observed transition onset locations are about the same (9.5 and about 11.2, respectively). These N-factor values are in the same range as found earlier for supersonic flight experiments and quiet tunnels. Hence, the results of the present study extend the applicability of the e^N method to high Mach number, chemically reacting flows.

Acknowledgments

This work was sponsored under NASA Contract NAS1-97020. Several members of High Technology Corp. technical staff, during the period of 1996–1999, contributed to various stages of the project. They include Chau-Lyan Chang, Venkit Iyer, Ray-Sing Lin, and Raja Sengupta.

References

[1]Smith, A. M. O., and Gamberoni, N., "Transition, Pressure Gradient, and Stability Theory," Douglas Aircraft Co., Inc., Rept. ES 26388, Long Beach, CA, 1956.

[2]Malik, M. R., "Stability Theory for Laminar Flow Control Design," *Viscous Drag Reduction in Boundary Layers*, edited by D. M. Bushnell and J. N. Hefner, Vol. 123, Progress in Astronautics and Aeronautics, AIAA, Washington, DC, 1990.

[3]Lees, L., and Lin, C. C., "Investigation of the Stability of the Laminar Boundary Layer in a Compressible Fluid," NACA TN 1115, 1946.

[4]Mack, L. M., "Boundary Layer Stability Theory," Jet Propulsion Lab., Rept. 900-277 rev. A, California Inst. of Technology, Pasadena, CA, 1969.

[5]Mack, L. M., "Review of Linear Compressible Stability Theory," *Stability of Time-Dependent and Spatially Varying Flows*, edited by D. L. Dwoyer and M. Y. Hussaini, Springer-Verlag, New York, 1987, pp. 164–187.

[6]Kendall, J. M., "Wind Tunnel Experiments Relating to Supersonic and Hypersonic Boundary-Layer Transition," *AIAA Journal*, Vol. 13, No. 3, 1975, pp. 290–299.

[7]Demetriades, A., "Hypersonic Viscous Flow over a Slender Cone; Part III: Laminar Instability and Transition," AIAA Paper 74-535, June 1974.

[8]Stetson, K. F., Thompson, E. R., Donaldson, J. C., and Siler, L. G., "Laminar Boundary Layer Stability Experiments on a Cone at Mach 8. Part 1: Sharp Cone," AIAA Paper 83-1761, June 1983.

[9]Malik, M. R., "Prediction and Control of Transition in Supersonic and Hypersonic Boundary Layers," *AIAA Journal*, Vol. 27, No. 11, 1989, pp. 1487–1493.

[10]Balakumar, P., and Malik, M. R., "Effect of Adverse Pressure Gradient and Wall Cooling on Instability of Hypersonic Boundary Layers," High Technology Corp., Rept. HTC-9404, Hampton, VA, 1994.

[11]Fedorov, A. V., Malmuth, N. D., Rasheed, A., and Hornung, H. G., "Stabilization of Hypersonic Boundary Layers by Porous Coatings," *AIAA Journal*, Vol. 39, No. 4, 2001, pp. 605–610.

[12]Chen, F.-J., Malik, M. R., and Beckwith, I. E., "Boundary-Layer Transition on a Cone and Flat Plate at Mach 3.5," *AIAA Journal*, Vol. 27, No. 6, 1989, pp. 687–693.

[13]Malik, M. R., "Instability and Transition in Supersonic Boundary Layers," *Laminar Turbulent Boundary Layers*, Fluids Engineering Div., Vol. 11, American Society of Mechanical Engineers, New York, 1984, pp. 139–147.

[14]Lachowicz, J. T., Chokani, N., and Wilkinson, S. P., "Boundary-Layer Stability Measurements in a Hypersonic Quiet Tunnel," *AIAA Journal*, Vol. 34, No. 12, 1996, pp. 2496–2500.

[15]Malik, M. R., "Transition in Hypersonic Boundary Layers," *Numerical and Physical Aspects of Aerodynamic Flows IV*, edited by T. Cebeci, Springer-Verlag, Berlin, 1990, pp. 321–331.

[16]Malik, M. R., and Anderson, E. C., "Real Gas Effects on Hypersonic Boundary-Layer Stability," *Physics of Fluids A*, Vol. 3, No. 5, 1991, pp. 803–821.

[17]Malik, M. R., "Stability Theory for Chemically Reacting Flows," *Laminar-Turbulent Transition*, edited by D. Arnal and R. Michel, Springer-Verlag, Toulouse, France, 1990, pp. 251–260.

[18]Stuckert, G. K., and Reed, H. L., "Linear Disturbances in Hypersonic, Chemically Reacting Shock Layers," *AIAA Journal*, Vol. 32, No. 7, 1994, pp. 1384–1393.

[19]Hudson, M. L., Chokani, N., and Candler, G. V., "Linear Stability of Hypersonic Flow in Thermochemical Nonequilibrium," *AIAA Journal*, Vol. 35, No. 6, 1997, pp. 958–964.

[20]Malik, M. R., Spall, R. E., and Chang, C.-L., "Transition Prediction in Hypersonic Boundary Layers," Sixth National Aero-Space Plane Symposium, Wright–Patterson AFB, OH, April 1989, Paper 67.

[21]Malik, M. R., Zang, T., and Bushnell, D., "Boundary Layer Transition in Hypersonic Flows," AIAA Paper 90-5232, April 1990.

[22]Carter, H. S., Raper, J. L., Hinson, W. F., and Morris, W. D., "Basic Measurements from a Turbulent-Heating Flight Experiment on a 5° Half-Angle Cone at Mach 20 (Reentry F)," NASA TM X-2308, 1971.

[23]Johnson, C. B., Stainback, P. C., Wicker, K. C., and Bony, L. R., "Boundary-Layer Edge Conditions and Transition Reynolds Number Data for a Flight Test at Mach 20 (Reentry F)," NASA TM X-2584, 1972.

[24]Sherman, M. M., and Nakamura, T., "Flight Test Measurements of Boundary-Layer Transition on a Nonablating 22-Degree Cone," *Journal of Spacecraft and Rockets*, Vol. 7, No. 2, 1970, pp. 137–142.

[25]Schneider, S. P., "Flight Data for Boundary-Layer Transition at Hypersonic and Supersonic Speeds," *Journal of Spacecraft and Rockets*, Vol. 35, No. 1, 1999, pp. 8–20.

[26]Anderson, J. D., Jr., *Hypersonic and High Temperature Gas Dynamics*, McGraw–Hill Series in Aeronautical and Aerospace Engineering, McGraw–Hill, New York, 1989, Chap. 17.

[27]Herbert, T., "Boundary-Layer Transition—Analysis and Prediction Revisited," AIAA Paper 91-0737, Jan. 1991.

[28]Li, F., and Malik, M. R., "Spectral Analysis of Parabolized Stability Equations," *Computers and Fluids*, Vol. 26, No. 3, 1997, pp. 279–297.

[29]Li, F., and Malik, M. R., "On the Nature of PSE Approximation," *Theoretical and Computational Fluid Dynamics*, Vol. 8, No. 4, 1996, pp. 253–273.

[30]Chang, C.-L., Malik, M. R., Erlebacher, G., and Hussaini, M. Y., "Compressible Stability of Growing Boundary Layers Using Parabolized Stability Equations," AIAA Paper 91-1636, June 1991.

[31]"GASP Version 3: The General Aerodynamic Simulation Program, Computational Flow Analysis Software for the Scientist and Engineer User's Manual," Aerosoft, Inc., Blacksburg, VA, 1996.

[32]White, W. B., Johnson, S. M., and Dontzig, G. B., "Chemical Equilibrium in Complex Mixtures," *Journal of Chemistry Physics*, Vol. 28, No. 5, 1958, pp. 751–762.

[33]Gupta, R. N., Yos, J. M., Thompson, R. A., and Lee, K.-P., "A Review of Reaction Rates and Thermodynamic and Transport Properties for an 11-Species Air Model for Chemical and Thermal Non-Equilibrium Calculations to 30,000∼K," NASA RP 1232, 1990.

[34]Blottner, F. G., Johnson, M., and Ellis, M., "Chemically Reacting Viscous Flow Program for Multi-Component Gas Mixtures," Sandia National Labs., SC-RR-70-754, Albuquerque, NM, Dec. 1971.

[35]Prabhu, D. K., Tannehill, J. C., and Marvin, J. G., "A New PNS Code for Chemical Nonequilibrium Flows," AIAA Paper 87-0284, Jan. 1987.

[36]Wilke, C. R., "A Viscosity Equation for Gas Mixtures," *Journal of Chemical Physics*, Vol. 18, No. 4, 1950, p. 517.

[37]Miner, E. W., Anderson, E. C., and Lewis, C. H., "A Computer Program for Two-Dimensional and Axisymmetric Nonreacting Perfect Gas and Equilibrium Chemically Reacting Laminar, Transitional and/or Turbulent Boundary Layer Flows," Virginia Polytechnic Inst. and State Univ., Rept. VPI-E-71-8, Blacksburg, VA, 1971.

[38]Hirschfelder, J. O., Curtiss, C. F., and Byron, B. R., *Molecular Theory of Gases and Liquids*, rev., Wiley, New York, 1967.

[39]Harris, J. E., and Blanchard, D. K., "Computer Program for Solving Laminar, Transitional, or Turbulent Compressible Boundary Layer Equations for Two-Dimensional and Axisymmetric Flow," NASA TM-83207, 1982.

[40]Krist, S. L., Biedron, R. T., and Rumsey, C. L., "CFL3D User's Manual," NASA TM-1998-208444, 1998.

[41]Garriz, J. A., Vatsa, V. N., and Sanetrik, M. D., "Issues Involved in Coupling Navier–Stokes Mean-Flow and Linear Stability Codes," AIAA Paper 94-0304, Jan. 1994.

[42]Zoby, E. V., and Rumsey, C. B., "Analysis of Free-Flight Laminar, Transitional, and Turbulent Heat-Transfer Results at Free-Stream Mach Numbers Near 20 (Reentry F)," NASA TM X-2335, 1971.

[43]Thompson, R. A., Zoby, E. V., Wurster, K. E., and Gnoffo, P. A., "An Aerothermodynamic Study of Slender Conical Vehicles," AIAA Paper 87-1475, June 1987.

[44]Wurster, K. E., Zoby, E. V., and Thompson, R. A., "Influence of Flowfield and Vehicle Parameters on Engineering Aerothermal Methods," AIAA Paper 89-1769, June 1989.

[45]Gnoffo, P. A., "A Vectorized Finite Volume, Adaptive Grid Algorithm Applied to Planetry Entry Problems, AIAA Paper 82-1018, June 1982.

[46]Tannehill, J. C., Ievalts, J. O., and Lawrence, S. L., "An Upwind Parabolized Navier–Stokes Code for Real Gas Flows," AIAA Paper 88-0713, Jan. 1988.

[47]Howard, F. G., "Thermal Analysis Methods and Basic Heat-Transfer Data for a Turbulent Heating Flight Experiment at Mach 20 (Reentry F)," NASA TM X-2282, 1971.

[48]Johnson, H. B., Seipp, T. G., and Candler, G. V., "Numerical Study of Hypersonic Reacting Boundary Layer Transition on Cones," AIAA Paper 97-2567, June 1997.

[49]Germain, P. D., and Hornung, H. G., "Transition on a Slender Cone in Hypervelocity Flow," *Experiments in Fluids*, Vol. 22. No. 3, 1997, pp. 183–190.

[50]Chang, C.-L., Vinh, H., and Malik, M. R., "Hypersonic Boundary-Layer Stability with Chemical Reactions Using PSE," AIAA Paper 97-2012, June 1997.

[51]Malik, M. R., Spall, R. E., and Chang, C.-L., "Effect of Nose Bluntness on Boundary Layer Stability and Transition," AIAA Paper 90-0112, Jan. 1990.

[52]Schneider, S. P., "Survey of Flight Data for Boundary-Layer Transition at Hypersonic and Supersonic Speeds," AIAA Paper 98-0432, Jan. 1998.

[53]Berkowitz, A. M., Kyriss, C. L., and Mertellucci, A., "Boundary Layer Transition Flight Test Observations," AIAA Paper 77-125, Jan. 1977.

[54]Robinet, J.-C., Gressier, J., Casalis, G., and Moschetta, J.-M., "Shock Wave Instability and the Carbuncle Phenomenon: Same Intrinsic Origin?," *Journal of Fluid Mechanics*, Vol. 417, 2000, pp. 237–263.

[55]Bushnell, D. M., "Notes on Initial Disturbance Fields for the Transition Problem," *Instability and Transition*, Vol. 1, edited by M. Y. Hussaini and R. G. Voigt, Springer-Verlag, New York, 1990, pp. 217–232.

[56]Stetson, K. F., Thompson, E. R., Donaldson, J. C., and Siler, L. G., "Laminar Boundary Layer Stability Experiments on a Cone at Mach 8, Part 2: Blunt Cone," AIAA Paper 84-0006, Jan. 1984.

[57]King, R. A., "Three-Dimensional Boundary-Layer Transition on a Cone at Mach 3.5," *Experiments in Fluids*, Vol. 13, 1992, pp. 305–314.

[58]Malik, M. R., and Balakumar, P., "Instability and Transition in Three-Dimensional Supersonic Boundary Layers," AIAA Paper 92-5049, Dec. 1992.

[59]Stetson, K. F., Thompson, E. R., Donaldson, J. C., and Siler, L. G., "Laminar Boundary Layer Stability Experiments on a Cone at Mach 8, Part 3: Sharp Cone at Angle of Attack," AIAA Paper 85-0492, Jan. 1985.

T. C. Lin
Associate Editor